

# Semidefinite Programming for Quantum Channel Learning

Mikhail Gennadievich Belov\*

*Lomonosov Moscow State University, Faculty of Mechanics and Mathematics,*

*GSP-1, Moscow, Vorob'evy Gory, 119991, Russia and*

*Autotech Group, Skolkovo Innovation Center, Nobel Street, Building 7, Moscow, 121205, Russia*

Victor Victorovich Dubov† and Vadim Konstantinovich Ivanov‡

*Peter the Great St. Petersburg Polytechnic University, 195251, Russia*

Alexander Yurievich Maslov § Olga Vladimirovna Proshina ¶ and Vladislav Gennadievich Malyshkin ||\*\*

*Ioffe Institute, Politekhnicheskaya 26, St Petersburg, 194021, Russia*

(Dated: December, 19, 2025)

\$Id: SemidefiniteProgrammingQuantumChannel.tex, v 1.135 2026/01/18 17:22:02 mal Exp \$

The problem of reconstructing a quantum channel from a sample of classical data is considered. When the total fidelity can be represented as a ratio of two quadratic forms (e.g., in the case of mapping a mixed state to a pure state, projective operators, unitary learning, and others), Semidefinite Programming (SDP) can be applied to solve the fidelity optimization problem with respect to the Choi matrix. A remarkable feature of SDP is that the optimization is convex, which allows the problem to be efficiently solved by a variety of numerical algorithms. We have tested several commercially available SDP solvers, all of which allowed for the reconstruction of quantum channels of different forms. A notable feature is that the Kraus rank of the obtained quantum channel typically comprises less than a few percent of its maximal possible value. This suggests that a relatively small Kraus rank quantum channel is typically sufficient to describe experimentally observed classical data. The theory was also applied to the problem of reconstructing projective operators from data. Finally, we discuss a classical computational model based on quantum channel transformation, performed and calculated on a classical computer, possibly hardware-optimized.

## I. INTRODUCTION

Knowledge representation is a crucial and distinctive feature in any Machine Learning (ML) technique. The form of the knowledge determines the degree of generalization a technique can exhibit. More generally, the form of knowledge representation can be considered as a computational framework. For example, ML techniques such as statistical learning [1], logical approaches [2], support vector machines [3], rules and decision trees [4], fuzzy logic [5, 6], and deep learning [7] can all be viewed as forms of computation. The learning process consists of building a model from the data, essentially solving a form of an inverse problem.

It is of special interest to relate computations to quantum mechanics. The most widely discussed form is to correspond a computational model to an actual quantum system, the time evolution of which would perform the computation (quantum computing). Another approach is to correspond a computational model to a quantum system, where knowledge representation is typically in the form of quantum channel mapping, which is then

computed on a classical computer. This paper considers the latter approach. The most general form of quantum evolution is a quantum channel, typically in the form of completely positive trace-preserving (CPTP) maps [8–11].

$$A^{OUT} = \sum_{s=0}^{N_s-1} B_s A^{IN} B_s^\dagger \quad (1)$$

The minimum number of terms in (1) is called the Kraus rank. For  $N_s = 1$ , it becomes a unitary quantum channel. The use of unitary operators for ML/AI knowledge representation has attracted attention recently [12–16].

In [17], we introduced the concept of the density matrix network, which considers a quantum channel as a classical computational model. Quantum channels, together with an auxiliary “tensor product” operator, can be combined in a network to perform arbitrary computations. The computational model takes a density matrix as input and produces a density matrix as output. The entire circuit can be considered as a flow of density matrix transformations. There is a clear meaning behind this transformation – namely, a quantum channel. The specific topology chosen is simply a matter of computational optimization. For smaller dimensions, the problem can always be optimized directly without assuming any particular topology. This contrasts with neural networks, where selecting the proper topology is a crucial factor for success. We approached the problem of reconstructing a quantum channel from data in [16], but encountered difficulties related to proxy fidelity when going beyond unitary learning. In this work, these

\* [mikhail.belov@tafs.pro](mailto:mikhail.belov@tafs.pro)

† [dubov@spbstu.ru](mailto:dubov@spbstu.ru)

‡ [ivvadim@rambler.ru](mailto:ivvadim@rambler.ru)

§ [maslov.ton@mail.ioffe.ru](mailto:maslov.ton@mail.ioffe.ru)

¶ [proshina.ton@mail.ioffe.ru](mailto:proshina.ton@mail.ioffe.ru)

\*\* [malyshki@ton.ioffe.ru](mailto:malyshki@ton.ioffe.ru)

difficulties are mostly overcome. Formally, the problem is to reconstruct a quantum channel, graphically depicted as a component

$$\rho \xrightarrow{\mathcal{Q}} \varrho \quad (2)$$

converting a density matrix  $\rho$  of dimension  $n_Q$  to a density matrix  $\varrho$  of dimension  $D_Q$  with the transformation (1); the IN/OUT lines in the circuits correspond not to a qubit, but to a density matrix of some dimension. The data is considered classical, and the transformation (1) is performed on a classical computer, possibly hardware-optimized. In this work, we consider the problem of reconstructing a quantum channel from a classical IN/OUT data sample.

In ML and AI, we typically have  $D \leq n$ , which means this is a “summarizing” quantum channel – it produces an output state of lower dimension than the input. One may also consider the opposite situation, where the output dimension is greater than the input. Such a quantum channel can be considered a “generative” one – it produces a state of higher dimension than the input. While for unitary learning different input/output dimensions create problems with trace-preservation constraints (which is why we explored partially unitary learning in [15]), quantum channels with a sufficiently high Kraus rank  $N_s$  can perfectly perform mappings between Hilbert spaces of different dimensions.

The paper is organized as follows. In Section II, we consider the problem of transforming classical vector-to-vector data into a wavefunction-to-wavefunction (or density-matrix-to-density-matrix) mapping. This is an important preliminary data-preparation step that enables an effective application of quantum channel transformations. In most existing work on unitary learning, authors simply normalize input and output vectors to unit norm and treat them as a form of “wavefunction”. We argue that this approach is insufficient, since in most cases it breaks gauge invariance. Suppose that the input and output vectors are transformed by two non-degenerate linear transformations. One should require that the resulting quantum channel be independent of the particular transformations chosen.

Then we consider possible criteria of closeness (fidelity) between the “quantum state” produced from a given input and the required “quantum state”. The choice of fidelity is a broad area of study [18–20]. A key requirement for our approach to be applicable is that the objective function be expressible as a quadratic function of the quantum channel mapping operators. For this reason, we restrict ourselves to input data in the form of mappings from mixed states to pure states. In this setting, the fidelity is exactly quadratic in the mapping operators (without approximation) and, at the same time, is sufficient for classical ML/AI input data passed through a quantum channel. The most general form of the fidelity to which our theory can be applied is given later in Eq. (34) as a ratio of two quadratic forms.

The transition from unitary learning to quantum channel learning allows us to distinguish between probabilistic mixtures of states and their superpositions.

In Section III, we formulate the quantum channel reconstruction problem as a constrained optimization problem. Two types of constraints are considered: trace preservation and unit-matrix preservation. The main result of this section is that, when considering a quantum channel of full Kraus rank  $N_s = \dim(IN) \dim(OUT)$ , the resulting optimization problem becomes an exact Semidefinite Programming (SDP) problem. A remarkable feature of this formulation is that the optimization problem is convex [21]. This allows the problem to be efficiently solved, for example, using polynomial-time interior-point algorithms. This is the main reason why we consider a quantum channel as a promising form of a classical computational model [17].

In Section IV, we demonstrate an application of SDP software to a number of quantum channel reconstruction problems. The SDP optimization allows for the reconstruction of quantum channels of different forms, from unitary to high Kraus rank. A noticeable feature is that the Kraus rank of the obtained quantum channel typically comprises less than a few percent of its maximal possible value. Low Kraus rank has deep significance in AI and ML applications: our numerical simulations show that a relatively small Kraus rank quantum channel is typically sufficient to describe experimentally observed classical data. SDP programming often shows superior results to our eigenvalue-based algorithm discussed in Appendix A, especially for high Kraus rank. A noticeable feature is that, even in unitary learning, the SDP convex optimization approach allows for the exact reconstruction of the unitary mapping, albeit at the cost of considering a much larger space of Choi matrices.

In Conclusion V, we summarize the results and discuss the perspectives of a quantum channel-based classical computational model arising from the convex form of the SDP quantum channel reconstruction problem. An important point is that a single large quantum channel can be split into a network of much smaller ones, connected in a hierarchical way, known as the density matrix network, which we introduced in Appendix C of [17]. This computational model is based on quantum channel transformation (1), performed and calculated on a classical computer, possibly hardware-optimized. The broad field of unitary learning, see [12–14], and thousands of subsequent works, has become an established field in ML and AI. Using a quantum channel is its natural extension. The low Kraus rank feature of quantum channels reconstructed from classical data makes them particularly similar.

## II. CLASSICAL DATA TRANSFORMATION VIA QUANTUM CHANNEL

For classical data, typically in the form of vector-to-vector mapping

$$\mathbf{x}^{(l)} \rightarrow \mathbf{f}^{(l)} \quad l = 1 \dots M \quad (3)$$

one needs to construct density matrix entities (in either pure or mixed state)

$$\rho^{(l)} \rightarrow \varrho^{(l)} \quad (4)$$

that can be passed through the quantum channel (2) to obtain the result  $\varrho$  from the input  $\rho$  with the highest possible fidelity. See [15, 17, 22] for examples of such conversions. In its simplest form, typical for ML problems, it takes the form of pure state to pure state mapping [17].

$$\frac{\sum_{j,k=0}^{n-1} x_j G_{jk}^{\mathbf{x};-1} x_k^{(l)}}{\sqrt{\sum_{j,k=0}^{n-1} x_j^{(l)} G_{jk}^{\mathbf{x};-1} x_k^{(l)}}} \rightarrow \frac{\sum_{j,k=0}^{D-1} f_j G_{jk}^{\mathbf{f};-1} f_k^{(l)}}{\sqrt{\sum_{j,k=0}^{D-1} f_j^{(l)} G_{jk}^{\mathbf{f};-1} f_k^{(l)}}} \quad (5)$$

Here, the  $x_k^{(l)}$  and  $f_j^{(l)}$  are the components of (3), and  $x_k$  and  $f_j$  are the components of the arguments of the wavefunctions

$$\psi^{(l)}(\mathbf{x}) \rightarrow \phi^{(l)}(\mathbf{f}) \quad (6)$$

The matrices  $G_{jk}^{\mathbf{x}} = \langle x_j | x_k \rangle$  and  $G_{jk}^{\mathbf{f}} = \langle f_j | f_k \rangle$  are Gram matrices calculated from  $\mathbf{x}^{(l)}$  and  $\mathbf{f}^{(l)}$  by averaging over the sample (3). The map in (5) is invariant with respect to arbitrary non-degenerate linear transformations of  $\mathbf{x}$  and  $\mathbf{f}$  in the original map (3). If the original map is given as  $d\mathbf{x} \rightarrow d\mathbf{f}$ , then a similar expression involving the Christoffel function can be used [23].

In this work, we consider sample data in the form of a mapping from a mixed state to a pure state.

$$\rho^{(l)} \rightarrow |\phi^{(l)}\rangle\langle\phi^{(l)}| \quad (7)$$

The reason we limit ourselves to this form is that, for our theory to be applicable, the total fidelity must be a quadratic function of the mapping operators  $B_s$ . The fidelity between a mixed state  $\varrho$ , obtained by passing an input state  $\rho$  through the quantum channel (2), and a pure state  $|\phi\rangle\langle\phi|$ , is given by the expected fidelity, as shown in Eq. (9.89) of Ref. [24], p.264:

$$F(|\phi\rangle\langle\phi|, \varrho) = \langle\phi|\varrho|\phi\rangle \quad (8)$$

For a general form of mapping (4), the quadratic fidelity is difficult to obtain, so a proxy (approximation) is required. In [16], we considered several forms of proxy fidelities and discussed their limitations. The problem of choosing an appropriate fidelity measure (objective function) is a broad area of study [18–20]. The key requirement

for our approach is that the objective function must be expressible as a ratio of two quadratic function of the mapping operators. We start by considering the weighted fidelity of individual state matches (8). The weights  $\omega^{(l)}$  are typically all equal to 1. In ML, the weights are sometimes adjusted to account for the importance of specific observations. The fidelity (8), summed over the sample (7), gives the total fidelity:

$$\mathcal{F} = \sum_{l=1}^M \omega^{(l)} \sum_{s=0}^{N_s-1} \langle\phi^{(l)}|B_s|\rho^{(l)}|B_s^\dagger|\phi^{(l)}\rangle \quad (9)$$

Expanding the parentheses yields an expression for  $S_{jk;j'k'}$ ; Eq. (11) is for pure state input  $\psi^{(l)}$ .

$$S_{jk;j'k'} = \sum_{l=1}^M \omega^{(l)} \phi_j^{(l)*} \phi_{j'}^{(l)} \rho_{kk'}^{(l)*} \quad (10)$$

$$S_{jk;j'k'} = \sum_{l=1}^M \omega^{(l)} \phi_j^{(l)*} \phi_{j'}^{(l)} \psi_k^{(l)*} \psi_{k'}^{(l)} \quad (11)$$

and the quadratic expression for the total fidelity (9)

$$\mathcal{F} = \sum_{s=0}^{N_s-1} \sum_{j,j'=0}^{D-1} \sum_{k,k'=0}^{n-1} B_{jk;s}^* S_{jk;j'k'} B_{j'k';s} \quad (12)$$

## III. QUANTUM CHANNEL RECONSTRUCTION PROBLEM

The problem of quantum channel reconstruction is reduced to the maximization problem (12), subject to constraints on  $B_s$ . The most typical constraints correspond to completely positive, trace-preserving (CPTP) mappings.

$$\delta_{kk'} = \sum_{s=0}^{N_s-1} \sum_{j=0}^{D-1} B_{jk;s}^* B_{jk';s} \quad (13)$$

For some ML problems, it is convenient to have an alternative form of constraint where a unit matrix is mapped to a unit matrix.

$$\delta_{jj'} = \sum_{s=0}^{N_s-1} \sum_{k=0}^{n-1} B_{jk;s}^* B_{j'k;s} \quad (14)$$

This form arises from partially unitary learning [15, 16] and corresponds to the condition for a quantum channel (1) to transform a unit input matrix  $A^{IN}$  into a unit output matrix  $A^{OUT}$ . This form does not preserve the trace and is primarily useful for exploring numerical algorithms and studying projections. This map is completely positive (CP) but not trace-preserving (TP) and should be treated accordingly. For a unitary mapping,  $N_s = 1$  and  $D = n$ , both forms of constraints coincide. Other forms of constraints can also be considered.

Additionally, an always-required constraint is that the mapping (1) must be a completely positive map. For the Kraus form, this condition is automatically satisfied.

An important feature of optimizing (12) subject to constraints (13) or (14) is that both the objective function and the constraints are quadratic functions of the mapping operators  $B_s$ . This optimization is referred to as a Quadratically Constrained Quadratic Program (QCQP). When  $N_s = 1$  and  $D = n$ , the problem of learning a unitary operator  $\mathcal{U}$  from mapping data is often referred to as “tomography of unitary operations” in quantum computation [25, 26], or “unitary learning” in artificial intelligence [13, 15]. In [15] we developed an iterative algorithm that, in most cases, provides the globally optimal solution to unitary learning. We then approached the problem of reconstructing a quantum channel from data in [16], but encountered difficulties related to proxy fidelity when going beyond unitary learning. In the present work, we re-approach this problem and show that, with the fidelity in the form of (12), or more generally (34), learning a full rank quantum channel is actually a simpler problem than learning unitary operators. This is the main motivation behind using a quantum channel as a classical computational model [17].

For numerical optimization the specific method of parametrizing of the space we learn the solution in, is typically the key to success. Besides working in the space of Kraus operators  $B_s$ , one may also consider an alternative in the form of the Choi matrix  $\mathcal{J}$ :

$$\mathcal{J}(\mathcal{E}) = \sum_{k,k'=0}^{n-1} |k\rangle\langle k'| \otimes \mathcal{E}(|k\rangle\langle k'|) \quad (15)$$

Where the quantum channel mapping  $\mathcal{E}$  is the mapping (1). The Choi matrix is constructed by mapping the basis states of the system to the corresponding output states under the channel. Each of the  $n \times n$  elements of the input space is mapped to a  $D \times D$  output matrix, resulting in a total size of  $Dn \times Dn$  elements. The Choi matrix is quadratic in the Kraus operators  $B_s$ . If we express the fidelity (12) and the constraints (13) or (14) in terms of the Choi matrix, these will become linear functions of its elements.

For the numerical method, it is convenient to define the Choi matrix in the form of swapped indices, specifically:

$$\mathcal{J}_{jk;j'k'} = \sum_{s=0}^{N_s-1} B_{jk;s}^* B_{j'k';s} \quad (16)$$

It has the same dimension  $Dn \times Dn$  as the tensor  $S_{jk;j'k'}$  and the original Choi matrix (15). The matrix  $\mathcal{J}_{jk;j'k'}$  is Hermitian when considering the  $jk$  pair as a multi-index  $\mathbf{i} = (j, k)$ , such that  $\mathcal{J}_{jk;j'k'} = \mathcal{J}_{j'k';jk}^*$ ; in numerical implementation, it is convenient to map the multi-index  $\mathbf{i}$  to a scalar index as  $i = jn + k$ . The quantum channel transformation (2) now takes a form similar to the partial

trace:

$$\varrho_{jj'} = \sum_{k,k'=0}^{n-1} \mathcal{J}_{jk;j'k'}^* \rho_{kk'} \quad (17)$$

The objective function (12) now is:

$$\mathcal{F} = \sum_{j,j'=0}^{D-1} \sum_{k,k'=0}^{n-1} \mathcal{J}_{jk;j'k'} S_{jk;j'k'} \quad (18)$$

The constraints (13) and (14), now take the partial trace forms (19) and (20) respectively

$$\delta_{kk'} = \sum_{j=0}^{D-1} \mathcal{J}_{jk;jk'} \quad (19)$$

$$\delta_{jj'} = \sum_{k=0}^{n-1} \mathcal{J}_{jk;j'k} \quad (20)$$

They are linear functions in the elements of  $\mathcal{J}_{jk;j'k'}$ . In SDP terms, the optimization problem becomes: Maximize (18) with respect to  $\mathcal{J}$ , subject to (19) (or (20)) constraints and the condition that  $\mathcal{J}$  is semidefinite,  $\mathcal{J} \succeq 0$ . If one considers the solution without the semidefinite constraint, imposing only the required linear constraints, the resulting linear-programming (LP) solution produces a matrix  $\mathcal{J}$  that generally has both positive and negative eigenvalues, and the obtained value of  $\mathcal{F}$  corresponds to the maximal eigenvalue of  $S$ . Whereas in the Kraus representation (1), the requirement for a completely positive map is automatically satisfied, for Choi matrix, an additional constraint of semidefiniteness is always required.

$$\mathcal{J} \succeq 0 \quad (21)$$

There are several possible forms in which to express this requirement. For example, it could be that  $\mathcal{J}$  is required to be the Gram matrix of some vectors:  $\mathcal{J}_{\mathbf{i};\mathbf{i}'} = \langle v^{[\mathbf{i}]} | v^{[\mathbf{i}']} \rangle$ . Alternatively, one may require  $\mathcal{J}$  to have only non-negative eigenvalues.

For the reconstruction of a quantum channel, the problem becomes: maximize the fidelity  $\mathcal{F}$  in the form (22)

$$\text{Tr} \mathcal{J} S \rightarrow \max \quad (22)$$

$$\text{Tr} \mathcal{J} A_c = \beta_c \quad c = 1 \dots N_c \quad (23)$$

subject to the constraints (23) and (21). The number of constraints  $N_c$  for (19) is  $n(n+1)/2$ , and  $D(D+1)/2$  for (20); the matrices  $A_c$  and scalars  $\beta_s$  are directly obtained from these. Without loss of generality, the matrices  $A_c$  and  $S$  can be taken to be Hermitian. Also, we will be studying only real symmetric matrices, which are required for ML and AI studies. In this form, the problem becomes exactly a Semidefinite Programming (SDP) problem. [27–32]. A remarkable feature of this formulation is that the optimization problem is convex [21]. SDP is defined as a special case of a conic-form convex optimization problem.

Specifically, when the cone is the cone of positive semidefinite matrices (the PSD cone), the resulting program is convex. The feasible set in an SDP is the intersection of an affine subspace (arising from equality constraints or affine linear matrix combinations) with the cone of positive semidefinite matrices — and this cone is convex. As a consequence, any local optimum is also a global optimum, and efficient polynomial-time interior-point algorithms exist, similar to those for LP. This is discussed in [21].

This explains why identifying a full rank quantum channel is a much simpler problem than unitary learning, which we previously considered [15]. The problem of unitary learning is non-convex. If we consider it as an SDP problem of above, the additional constraint that  $\mathcal{J}$  be a rank-one matrix must be imposed, in addition to the requirement  $\mathcal{J} \succeq 0$ . The technique developed in [15] includes a major transition from traditional mathematical analysis tools [13, 14, 30, 31] (e.g., gradient, derivative, etc.) to using algebraic tools (eigenproblem); this greatly increases the chances of finding the global maximum. This technique can also be applied to the quantum channel; the difficulties we encountered in [16] were mostly overcome by properly selecting the basis used to represent the quantum channel (see Appendix A below).

However, the problem of full rank quantum channel reconstruction appears to be much simpler — a convex SDP problem — as long as the fidelity (12) takes the quadratic form in the mapping operators, or more generally, as a ratio of two quadratic forms (34). For this reason, we approach it using interior-point SDP optimization software [33–35]. We also consider it using the updated version of our algorithm [16], see Appendix A. The main strength of our algorithm is its applicability to non-convex problems. For example, if we seek a solution as a quantum channel of a specific Kraus rank  $N_s$ , the problem becomes non-convex and significantly more difficult to approach. While our algebraic approach is fully applicable to non-convex problems (such as unitary learning), it is significantly less computationally efficient than interior-point SDP optimization methods for convex problems. This difference in computational efficiency becomes especially significant in the case of high Kraus-rank quantum channels, particularly the full-rank ones.

#### IV. PRACTICAL DEMONSTRATIONS OF QUANTUM CHANNEL RECONSTRUCTION FROM DATA

In this section, we examine several quantum channel reconstruction problems employing different methods. We begin with the simplest case of a unitary mapping.

##### A. Reconstructing Unitary Mappings from Data

Whereas in most practical ML/AI problems the data is given in the form of a general vector-to-vector map-

ping (3), which must first be converted into a wavefunction mapping such as (5), unitary dynamics does not require this step, since the data are already provided in wavefunction-mapping form. Consider a simple classical problem discussed in [15]. Let there be an initial state vector  $\mathbf{X}^{(0)}$  with unit  $L^2$  norm, and a unitary matrix  $\mathcal{U}$ . The operator  $\mathcal{U}$  is applied to  $\mathbf{X}^{(0)}$   $M$  times:

$$\mathbf{X}^{(l+1)} = \mathcal{U}\mathbf{X}^{(l)} \quad (24)$$

From this sequence, we construct  $M$  observation pairs  $(\psi^{(l)}, \phi^{(l)})$  by selecting the  $(l, l+1)$  elements of the sequence and multiplying them by random phases  $\exp(i\xi_l)$  and  $\exp(i\zeta_l)$  (or by  $\pm 1$  in the real-valued case).

$$|\psi^{(l)}\rangle = \exp(i\xi_l) |\mathbf{X}^{(l)}\rangle \quad (25a)$$

$$|\phi^{(l)}\rangle = \exp(i\zeta_l) |\mathbf{X}^{(l+1)}\rangle \quad (25b)$$

The mapping then coincides exactly with (7), with  $\rho^{(l)} = |\psi^{(l)}\rangle\langle\psi^{(l)}|$  and  $\varrho^{(l)} = |\phi^{(l)}\rangle\langle\phi^{(l)}|$ . The random phases render standard regression-type methods inapplicable; however, the tensor  $S_{jk;j'k'}$  in (11) has all random phases cancelled.

The sample (24) should be information-complete [36]. For example, if  $\mathcal{U}$  corresponds to a Hamiltonian  $H$ ,

$$\mathcal{U} = \exp\left[-i\frac{\tau}{\hbar} H\right] \quad (26)$$

and  $\mathbf{X}^{(0)}$  is an eigenvector of  $H$ , then every step of the mapping (24) is reduced to multiplying  $\mathbf{X}$  by a phase. In this numerical experiment, we select  $\mathbf{X}^{(0)}$  at random, so that the unitary dynamics (24) involves all eigenvectors of the corresponding Hamiltonian.

The tensor  $S_{jk;j'k'}$  (11) is obtained from these  $M$  observations, and we use it to reconstruct  $\mathcal{U}$ . Whereas in [15] we sought  $\mathcal{U}$  specifically among unitary operators ( $N_s = 1$ ), here we consider the following two cases:

- A full-rank ( $N_s = n^2$ ) quantum channel (1) using interior-point SDP optimization software [33–35]. This problem is convex and is expected to be efficiently solvable. SDP optimization yields the Choi matrix (16). When the solution is recovered exactly, this matrix has rank one, and the unitary operator  $\mathcal{U}$  can be obtained from its corresponding eigenvector.
- A quantum channel (1) of specific rank  $N_s \geq 1$  using the updated version of our algorithm from Appendix A. This problem is non-convex, as the quantum channel is not full-rank, but our algebraic approach is typically capable of finding the global maximum. This optimization problem yields the quantum channel in the  $LL^T$  representation (A1). When the solution is recovered exactly, the matrix  $B$  (A4) of dimension  $Dn \times N_s$  has a single nonzero column, which corresponds to the desired unitary operator  $\mathcal{U}$ .

The purpose of this section numerical experiments is to assess how well the new technique can handle the well-established problem of unitary learning, specifically reconstructing unitary channels (Kraus rank one,  $N_s = 1$ ) using a quantum channel with a much higher Kraus rank.

Here we reproduced the unitary dynamics ( $N_s = 1$ ,  $D = n$ ) results of Section IV of [15] using the following software:

- CVXPY 1.7.5 SDP optimization software [35] from [www.cvxpy.org](http://www.cvxpy.org). It was installed as `pip3 install cvxpy` and then integrated into our Java codebase with a script `com/polytechnik/sdpeexternalsolvers/solver_cvxpy.py`, which has a `json` file input/output interface implemented in `com/polytechnik/sdpeexternalsolvers/CVXPYsolver.java`; this requires `Gson` library to be installed.
- SDPA 7.3.20 SDP optimization software [33] from [sdpa.sourceforge.net](http://sdpa.sourceforge.net). It was compiled to OS-native code and then integrated into our Java codebase with the JNI implementation `com/polytechnik/sdpeexternalsolvers/SDPAsolver.java`.
- An updated version of our algebraic approach algorithm, as described in Appendix A, is implemented in `com/polytechnik/kgo/QCIverseProblem.java`.

The reconstruction was tested on unitary dynamics data of the form (24), so no preliminary conversion, such as (5), is required. In these tests, we have a known unitary operator  $\mathcal{U}$  that generates an information-complete data sample (25), from which the tensor  $S_{jk;j'k'}$  (11) is created. While the algorithm from Appendix A finds the unitary operator directly, the SDP optimization software finds the Choi matrix (16). The unitary operator  $\mathcal{U}$  is then obtained from  $\mathcal{J}_{jk;j'k'}$  as its eigenvector, corresponding to the maximal eigenvalue.

The results for SDP software CVXPY and SDPA are presented in Fig. 1. The unitary mapping exact reconstruction results from [15] were reproduced with the software in question. The simulation results can be summarized as follows. For small  $n$ , the algorithm from Appendix A is typically faster, as it works in a space of  $\text{dim}_1$  (A7) parameters, whereas the SDP algorithms work in a space of the Choi matrix with dimension  $n^2 \times n^2$ . If one attempts to put an explicit constraint on the rank of the Choi matrix (which is equal to one in the case of unitary learning), this makes the problem non-convex and not directly solvable with SDP software. However, the mentioned SDP software was able to find the rank-one Choi matrix exactly for sufficiently large  $n$ , without an explicit constraint on the Choi matrix rank. For a 16-core 5GHz x64 CPU with 32GB of memory, CVXPY has a maximum  $n$  of about 22 (Choi matrix of dimension  $484 \times 484$ ), and is limited by the calculation time. For SDPA, the maximum  $n$  is about 50 (Choi matrix of dimension  $2500 \times 2500$ ), and is typically limited by memory. The algorithm from Appendix A is limited by the eigenproblem dimension

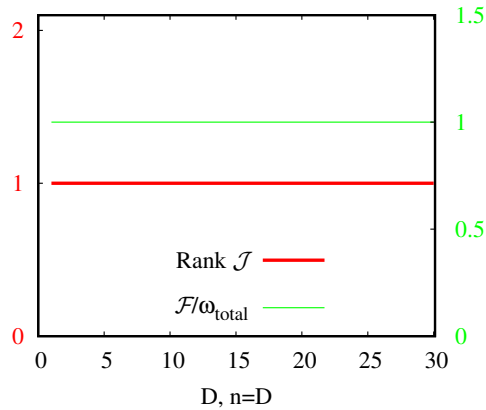


FIG. 1. The rank of the Choi matrix  $\mathcal{J}$  (16) (red), obtained as a solution to the optimization problem (22) for unitary mapping (25) data, is shown. This plot demonstrates a perfect reconstruction of the unitary operator from the data for the dimension range  $1 \leq D = n \leq 30$ . We made similar plots in [15] using our original software. The presented plot was generated using the off-the-shelf SDP software: CVXPY and SDPA, both of which reconstruct the unitary channel exactly. The fidelity (green) of the reconstructed channel is exact because the quantum channel was reconstructed perfectly, and the original unitary mapping maps a pure state to a pure state (24), yielding the exact fidelity (12). The purpose of this plot is to demonstrate the application of the convex SDP optimization approach to the problem of unitary learning.

(A7). Note that most regular commercial software uses `int32` array indices, which limits the use of matrices with dimensions larger than  $\sqrt{2^{31}} \times \sqrt{2^{31}}$ , i.e.,  $46340 \times 46340$ . For larger matrices, all the libraries must be recompiled with `int64` array indices.

We conclude that, for unitary dynamics data, the SDP optimization allows for the exact identification of the unitary dynamics, despite this being a difficult case of a rank-one Choi matrix. There was no failure in SDP reconstruction of the thousands of randomly generated unitary matrices we tried, in addition to those from [15]. These numerical experiments show that the convex nature of the SDP optimization problem makes the difficulties mostly technical, which can be overcome with algorithm improvements and possibly with hardware optimization.

## B. Toy Example in Quantum Channel Reconstruction

Before we consider applications for the practical reconstruction of a quantum channel, it would be convenient to first examine the quantum channels that allow for achieving 100% fidelity in pure state mapping. When the fidelity is exact, this greatly simplifies the assessment of algorithm correctness and sensitivity to problem degeneracy.

A pure-to-pure state mapping would not give 100% fidelity for a general CPTP quantum channel, except for unitary channels and quantum channels with  $N_s = 1$  and

$D \geq n$  that satisfy the trace preserving constraints.

In this section, we consider a CPTP quantum channel with  $D > n$  that satisfies (13). This channel has Kraus rank one, preserves the trace, and is not unitary. To some extent, it is similar to partially unitary channels with  $D < n$  satisfying (14) that we considered in [15].

These forms have Kraus rank one and computational properties similar to the unitary optimization considered in the previous section. To construct such a channel, we randomly generated  $B_{jk;s}$  operators, now with  $D > n$ . These are actually the operators  $B_{jk;s}$  from Appendix A, but without the lower-diagonal condition (A4). Using the transform (A24), we obtain the  $\tilde{B}_{jk;s}$  operators that satisfy the trace-preservation constraint (13). Then, we randomly generated a wavefunction  $\psi^{(l)}$ , and calculated  $\phi^{(l)}$  by passing it through the quantum channel. The rest is similar to the unitary optimization above: we constructed the tensor  $S_{jk;j'k'}$  (11) and solved the optimization problem using the same software as for the unitary learning above.

The results are the following. The CVXPY and Appendix A software were able to always exactly reconstruct the original  $D > n$  quantum channel used to construct the sample. The SDPA often misidentifies the problem as being unbounded and frequently fails to find the solution; this can, to some extent, be resolved by adjusting the parameter `lambdaStar`. Overall, the results are very similar to those of the unitary learning case above, where SDP optimization is limited by the dimension of the Choi matrix, and the Appendix A software is limited by the dimension of the eigenproblem (A6). The purpose of this toy-channel example is to present a simple, non-unitary quantum channel that can be reconstructed exactly.

### C. Reconstructing Quantum Channel Mappings from Data

Whereas unitary learning, is an established field of ML and AI, the application of general quantum channel mapping (1) to ML and AI represents a novel form of knowledge representation, allowing one to distinguish between probabilistic mixtures of states and their superposition. We approached this representation with an eigenproblem-based algorithm back in [16, 17], but some problems still remain, as discussed in Appendix A 2 below.

The convex nature of the SDP problem offers a new perspective on the direct reconstruction of quantum channel mappings from experimental data. The only important limiting factor here is the requirement for fidelity to be a ratio of two quadratic function of the mapping operators. When a proxy fidelity (approximation) is used to build a quadratic form, the maximum of the proxy fidelity may not be achieved for the original quantum channel. In Table I of [16], we demonstrated, for a Kraus rank-3 quantum channel, a situation where a single unitary operator provides a higher proxy fidelity than the proxy fidelity of the entire rank-3 quantum channel. For true fidelity,

the situation is the opposite: the fidelity of the rank-3 quantum channel is 100%, and any unitary operator gives a much lower fidelity. This makes the selection of the specific form of fidelity a crucial factor in quantum channel reconstruction.

However, this is typically not an issue in the ML and AI fields, where vector-to-vector mapping (3) is usually converted to pure state mapping, such as (5), allowing the use of quadratic fidelity in mapping operators (8). At the same time, for a pure state-to-pure state mapping, a quantum channel that provides 100% fidelity for pure state mapping may not exist, which complicates the evaluation of the quality of the solution obtained. If we find the solution, how can we prove that it is the optimal one? One simple method is to use several different software packages and compare the results.

A general quantum channel (1) mapping mixed states (4) requires the fidelity between the obtained  $\varrho$  and the desired  $\sigma$  density matrices, as described in [37] p. 409, [24] p. 285,

$$F(\sigma, \varrho) = \left| \text{Tr} \sqrt{\varrho^{1/2} \sigma \varrho^{1/2}} \right|^2 \quad (27)$$

instead of the familiar expression in Eq. (8), which gives a quadratic total fidelity (9) in the mapping operators  $B_s$ . Preferably, we would like to have the  $\sigma, \varrho$  states that allow us to write the fidelity as

$$F(\sigma, \varrho) = \text{Tr} \sigma \varrho \quad (28)$$

in order to obtain the quadratic expression (12) with the tensor

$$S_{jk;j'k'} = \sum_{l=1}^M \omega^{(l)} \varrho_{jj'}^{(l)*} \rho_{kk'}^{(l)*} \quad (29)$$

However, (28) matches (27) only when one of the density matrices,  $\sigma$  or  $\varrho$ , is a pure state. This particularly explains why the form in (8) is sufficient in most ML and AI classical applications, where the desired density matrix  $\sigma$  is a pure state, typically obtained from a vector-to-vector mapping (3) in a manner similar to (5).

#### 1. Low Choi Matrix Rank as an Intrinsic Feature of Optimization Solutions

We start with the task of identifying the Choi matrix structure. First, a large sample  $M \gg Dn$  of wavefunctions (6) was randomly generated for various values of  $D$  and  $n$ . The case  $D < n$  is typically more important in practical applications, for example as a feature-identification task. After the computation of the tensor  $S_{jk;j'k'}$  (29), the optimization problem is solved. The matrix  $S_{jk;j'k'}$  generated in the described way is non-degenerate, with eigenvalues approximately more or less evenly distributed within some range. Effectively, this is a random matrix obtained as a fourth-degree correlator of two vectors  $\psi$  and  $\phi$  (11), with the vectors now chosen randomly.

The optimization is approached with the SDP algorithm to solve the optimization problem (22) subject to the TP constraints (19) and CP constraints (21). The solution results in the Choi matrix (16) being obtained. The CVXPY and SDPA software perform quite well for this task; SDPA is faster and gives better precision, but sometimes misidentifies the problem as being unbounded. Our Appendix A software has some other issues, which are discussed below in section A 2.

Having these tools available, the first question to ask is about the rank of the obtained Choi matrix. When fitting random data using traditional learning representations, such as least squares, PCA, neural networks, and others, for random input/output data, the information typically propagates to all available degrees of freedom of the model. Numerical experiments show that this does not seem to be the case for quantum channel mapping: The obtained Choi matrix typically has a rank much lower than its maximal possible rank  $Dn$ . To identify the Choi matrix structure, we performed the following numerical experiment:

For a given  $n$  and  $D$ , we randomly generate  $M = 2n^2D^2 + 100000$  normalized wavefunction pairs as pseudo-random unit-norm vectors of length  $n$  ( $\psi^{(l)}$ ) and  $D$  ( $\phi^{(l)}$ ), considering them as if they were the mapping (6). Here and below, the phrase “generated random matrix/vector” refers to using a  $[-1 : 1]$  uniformly distributed pseudo-random generator, `java.util.Random`, with a specific initial random value set to allow reproduction of the numerical experiment. From the obtained mapping, we construct the tensor  $S_{jk;j'k'}$  (11) and solve the optimization problem with it. The result of the optimization yields the Choi matrix (16) of dimension  $Dn \times Dn$ . All the eigenvalues of the Choi matrix are obtained. Many of them are small, making it difficult to distinguish actually small values from those due to numerical errors. For this reason, we define the rank of the Choi matrix as follows: for sorted eigenvalues, going down from the largest ( $i = Dn - 1$ ) to the smallest ( $i = 0$ ), we stop when either the eigenvalue is lower than  $10^{-5}$  or the ratio to the previous eigenvalue  $\lambda^{[i+1]}/\lambda^{[i]}$  exceeds  $10^4$ .

In Fig. 2, the rank of the obtained Choi matrix as the solution for optimization problem with this  $S_{jk;j'k'}$ , corresponding to a completely random mapping (not corresponding to an actual quantum channel), is presented for two cases: equal IN/OUT dimensions  $1 \leq D = n \leq 30$ , and for fixed  $n = 15$  with varied  $1 \leq D \leq 30$ . The optimization problem was solved by CVXPY and SDPA programs. They typically produce almost identical solutions with identical ranks, with only a few cases of noticeable differences. As expected, the Choi matrix rank almost does not depend on the initial random value used to generate random mapping (6) – only in a few points the Choi matrix rank may possibly differ by one, so we present the result for a single realization of pseudo-random sample, as there is no need to average over different runs.

The most unexpected result is that the rank of the Choi matrix, corresponding to the optimization problem solution with  $S_{jk;j'k'}$ , which is obtained as a four-particle

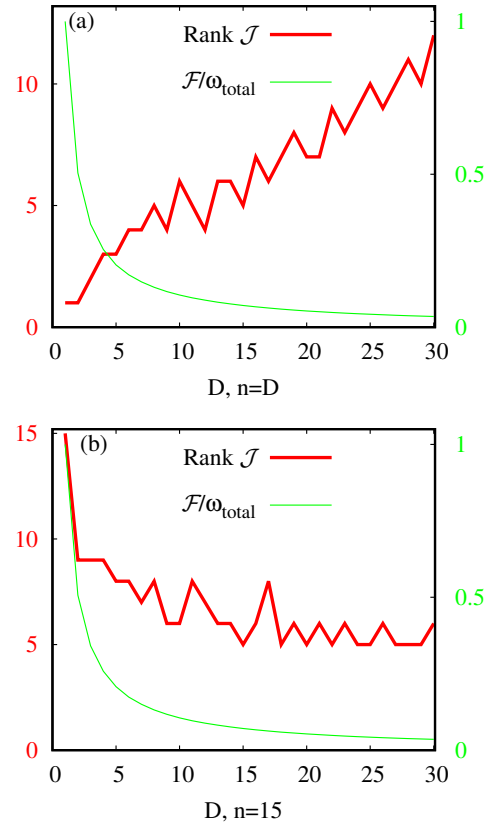


FIG. 2. The rank of the Choi matrix  $\mathcal{J}$  (16) (red) obtained as a solution to the optimization problem for a random  $\psi \rightarrow \phi$  mapping (6): (a) The case  $1 \leq D = n \leq 30$ . The rank grows slowly with the increase of  $n$ ; the rank value typically comprises less than 1.5% of the matrix dimension  $Dn$ . (b) The case where  $n = 15$  is fixed and  $1 \leq D \leq 30$  is varied. The maximal obtained Choi matrix rank is 15 for  $D = 1$  (trace calculation); the rank decreases slowly with an increase in  $D$ . The green line represents relative fidelity  $\mathcal{F}/\sum_l \omega^{(l)}$ . Since the sample is random, the fidelity decreases with the increase in problem size, as it becomes less likely for two random states to match as the dimension increases. For  $D = 1$ , the fidelity is exact:  $\mathcal{F} = \sum_l \omega^{(l)}$ ; this is simply a trace calculation. These plots show that it is difficult to obtain a high-rank Choi matrix as the solution to the quantum channel reconstruction optimization problem. Quantum channels reconstructed from classical data usually exhibit a low Kraus rank.

correlation  $\langle \phi_j^* \phi_{j'} \psi_k^* \psi_{k'} \rangle$  (11) of random wavefunction, is small. For example, Fig. 2a shows that the rank of the Choi matrix does not exceed 12 for  $D = n = 30$ , i.e. it is less than 1.5% of the matrix dimension. This is quite unusual. We compare this case with a general case of a random  $B_{jk;s}$ : we generated an initial random matrix  $B_{jk;s}$  of  $N_s = Dn$ , converted it to trace-preserving form (13) with the transform (A24), then obtained the corresponding Choi matrix (16), and finally determined its rank. Whereas for the Choi matrix obtained as a solution to the optimization problem, the rank is typically small, the rank of the Choi matrix obtained from this randomly

generated  $B_{jk;s}$  is very close to the maximal possible rank  $Dn$ , typically equal to or differing by no more than  $2 - 3$  from the maximal value.

In Fig. 2b, we fixed  $n = 15$  and varied  $1 \leq D \leq 30$ . At  $D = 1$ , the rank is maximal, 15, which corresponds to a quantum channel performing a trace calculation, as in Eq. (1), with  $B_s$  being an arbitrary orthogonal basis. As  $D$  increases, the rank of the Choi matrix decreases. The fidelity (green line) also decreases with the increase in problem size, as it becomes less likely for two random states to match as the dimension increases.

These numerical experiments show that quantum channels reconstructed from classical data typically exhibit a low Kraus rank. This is an important feature to consider when using quantum channels as ML/AI knowledge representations. It will be shown below that this result of a low-rank Choi matrix is common and occurs not only for randomly generated mappings. The random mapping is the most representative: if it were a linear regression or PCA-type expansion, it would expand to all available degrees of freedom. A question arises as to whether the low Kraus rank (about a few percent of the matrix dimension) of the solution  $\mathcal{J}$  to the optimization problem (22) is a specific feature of the  $S_{jk;j'k'}$  form obtained from “classical” data, as four-particle correlation in (11), or if it is an intrinsic property of the optimization problem itself.

The simplest test would be to consider  $S_{i;i}$  as a random Hermitian matrix with multi-index  $i = (j, k)$ , without any relation to four-particle correlation as in (11) or (29), and solve the optimization problem with it as if it were the tensor  $S_{jk;j'k'}$ . The result for random matrix in Fig. 3 is very similar to what we observed for the random sample in Fig. 2. Both CVXPY and SDPA produce identical solutions. This fact – that a random  $S_{i;i}$ , without any internal structure, produces a solution to optimization problem (22) with a low-rank Choi matrix  $\mathcal{J}$  – leads us to conclude that the low rank of the solution is an intrinsic property of the optimization problem (22), and is not related to the way the sample is constructed or how  $S_{jk;j'k'}$  is calculated (29).

These findings are also supported by testing the reconstruction of quantum channels that we consider below. Additionally, we tried a variety of other forms of  $S_{jk;j'k'}$  and have never been able to obtain a Choi matrix solution to (22) with a rank greater than  $\max(D, n)$ . The fact that, for quantum channel reconstruction, the optimization problem solution typically produces a low-rank Choi matrix is an important property in practice. Low Kraus rank has deep significance in AI and ML applications: our numerical simulations show that a relatively small Kraus rank quantum channel is typically sufficient to describe experimentally observed data. This allows the use of a wide range of problem optimizations, particularly hardware-type optimizations. Most importantly, quantum channel learning representation can be considered a natural extension to unitary learning; the convex nature of the optimization problem makes the approach especially appealing in practical applications.

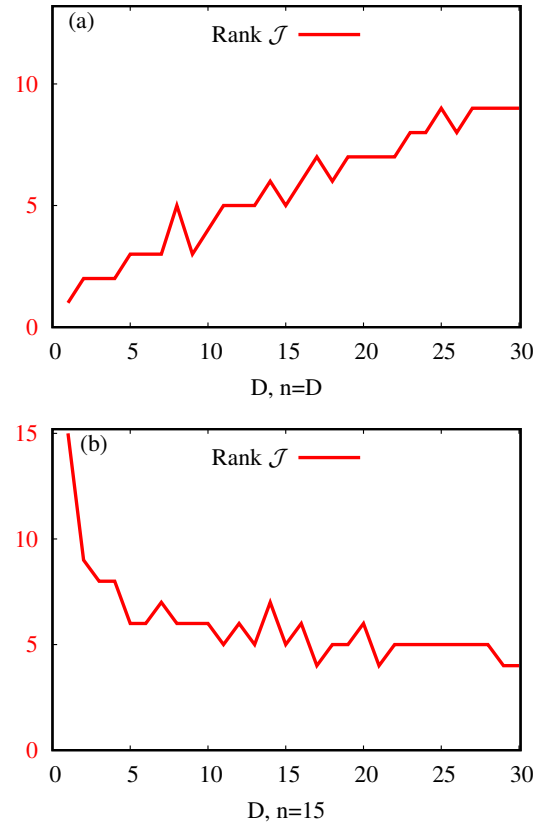


FIG. 3. The rank of the Choi matrix  $\mathcal{J}_{i;i'}$  (16) obtained as a solution to the optimization problem for a case with random  $S_{i;i'}$ , without any internal structure, is shown. Similarly to Fig. 2, we also obtain a low-rank Choi matrix  $\mathcal{J}$ . This leads us to conclude that the low rank of the solution (a few percent of the matrix size  $Dn$ ) is an intrinsic property of the optimization problem (22).

## 2. Data-Driven Quantum Channel Reconstruction

After establishing the important property of low Choi rank in the optimization problem solution, we test the approach on some actual data. The main difficulty is that there is no quantum channel (except for unitary and unitary-like channels) that will map pure states (6) exactly. For this reason, for a general quantum channel, we construct a sample that transforms an input pure state  $\psi^{(l)}$  to an output mixed state  $\varrho^{(l)}$  by passing  $\psi^{(l)}$  through the channel, and then use the eigenvector of the output state  $\varrho^{(l)}$  corresponding to the maximal eigenvalue as the resulting pure state  $\phi^{(l)}$ . In this way, the quantum channel reconstruction problem can be approached directly, but the original quantum channel can serve only as a lower-bound estimate for the solution. Specifically:

- We construct full Kraus rank ( $N_s = Dn$ ) operators  $B_{jk;s}$  as random matrices with  $D, n = 1 \dots 30$ . This is a completely positive but not necessarily trace-preserving map from a space of dimension  $n$  to a space of dimension  $D$ . Using the transform (A24),

we obtain the  $\tilde{B}_{jk;s}$  operators that satisfy the trace-preserving constraint (13); these are actually the operators  $B_{jk;s}$  from Appendix A, but without the lower diagonal condition (A4). As discussed above, the Choi matrix corresponding to this randomly generated quantum channel has a Kraus rank equal to or very close to the maximal value,  $Dn$ .

- For  $l = 1 \dots M$ , where  $M$  is chosen as  $M = 2n^2D^2 + 100000$ , we randomly create wavefunctions  $\psi^{(l)}$  of dimension  $n$ . The state  $|\psi^{(l)}\rangle\langle\psi^{(l)}|$  is then passed through the quantum channel (1), and the density matrix  $\rho^{(l)}$  of dimension  $D$  is obtained. The mixed-state output  $\rho^{(l)}$ , however, does not allow the quadratic fidelity (8) to be applied. To obtain the mapping of the form (7), we find all eigenvectors of  $\rho^{(l)}$  and select  $|\phi^{(l)}\rangle$  as the one corresponding to the maximal eigenvalue of  $\rho^{(l)}$ . (Note that for a large  $M$ , this construction of a sample can be slow, but reducing the sample size  $M$  does not change the result). This way, the pure state-to-pure state mapping with quadratic fidelity (9) is obtained, and the tensor  $S_{jk;j'k'}$  (11) is calculated. This tensor, however, does not correspond to the quantum channel used to construct the sample, as the sample was modified to fit the pure state-to-pure state paradigm, which is typical in the data analysis field. Thus, we cannot require the reconstructed channel to match the original quantum channel exactly, but we can compare the fidelity obtained, using the original quantum channel as a lower bound.

This analysis was conducted using **CVXPY** and **SDPA** software, which produce identical results. The difficulties with our eigenproblem-based approach are discussed in Appendix A 2 below. The result is presented in Fig. 4 in the same form as in Fig. 2 for the random sample. The  $\mathcal{F}_{init}$  (green) is the fidelity obtained for the pure state-to-pure state sample, with the quantum channel initially used to construct the sample by taking the eigenvector corresponding to the highest eigenvalue of the output density matrix  $\rho^{(l)}$ . It decreases with the dimension, but slower than in Fig. 2 for the random sample. The  $\mathcal{F}$  (olive) is the fidelity corresponding to the quantum channel obtained as the solution to the optimization problem (22) with the sample we created. At high dimensions, it exceeds  $\mathcal{F}_{init}$  by several times. This simulation confirms an important feature of the low Kraus rank of the resulting Choi matrix.

Whereas we cannot theoretically confirm that the found solution is exactly optimal, the identical results obtained from **CVXPY** and **SDPA** software, along with the convexity property of the SDP problem itself, lead us to conclude that the practically found fidelity maximum is global. These simulations confirm the applicability of the SDP technique to quantum channel reconstruction and show that a quantum channel with a relatively small Kraus rank is typically sufficient to describe experimentally observed data.

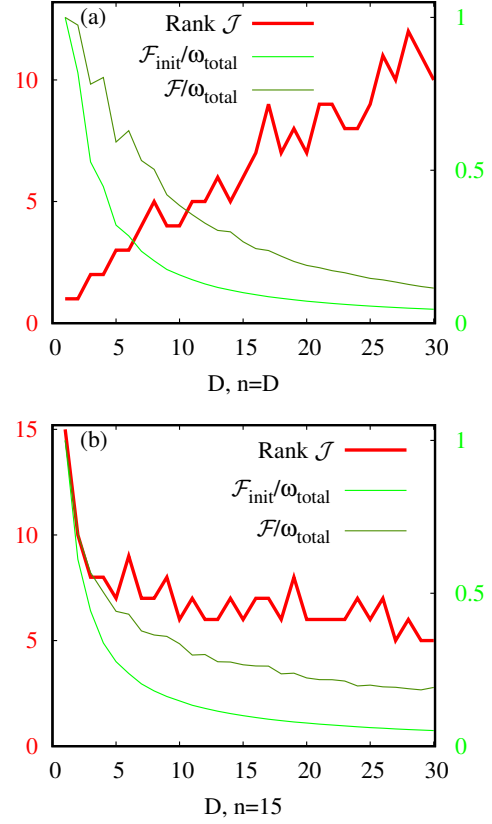


FIG. 4. The rank of the Choi matrix  $\mathcal{J}$  (16) (red) obtained as a solution to the optimization problem for a sample calculated as a random pure state passed through the quantum channel, with the eigenvector corresponding to the maximal eigenvalue of the output density matrix taken as the result. The fidelity  $\mathcal{F}_{init}/\sum_l \omega^{(l)}$  (green) is the fidelity of this initial map on the generated sample. The fidelity  $\mathcal{F}/\sum_l \omega^{(l)}$  (olive) is the fidelity of the quantum channel obtained as a result of the optimization problem (22) with  $S_{jk;j'k'}$  (11) from this sample. At high dimensions, it is several times higher than the fidelity of the original map. The low Kraus rank feature is also confirmed for this sample. (a) The case  $1 \leq D = n \leq 30$ . (b) The case where  $n = 15$  is fixed and  $1 \leq D \leq 30$  is varied. When  $D = 1$ , trace preservation reduces to the trace-calculating quantum channel, which has Kraus rank  $N_s = n$ .

#### D. Approximate Inverse of a Quantum Channel

Consider a CPTP map (1) subject to the TP constraints (13), and ask under what conditions this channel can be inverted. An invertible quantum channel is one whose action can be undone by another CPTP map. This requirement is very restrictive. A quantum channel is invertible (i.e., admits a CPTP inverse) if and only if it is a unitary channel. This corresponds to physical reversibility with no loss of information. In all other cases, one can obtain only one of the following weaker notions of invertibility:

- A linear inverse, which may exist as a linear map but is not necessarily completely positive.

- An inverse on a restricted set of states, for example, one defined on a known subspace.
- An inverse with post-selection, which may be linear but is not necessarily trace-preserving.
- An approximate inverse, in which some irreversibility error remains.

It is important to note that for pure state-to-pure state mapping, the fidelity in the form (8) gives exactly the same  $S_{jk;j'k'}$  (11) for both the direct and inverse quantum channels, with the indices swapped. Note that the trace-preserving constraints (13) are the same as the unit matrix invariance constraint (14), with the indices swapped. Thus, the maximization of the fidelity (12) subject to the (13) constraint gives the direct quantum channel, and the maximization of the same fidelity subject to (14) gives the inverse quantum channel. This follows immediately from swapping  $A^{IN}/A^{OUT}$  in (1) and applying the trace-preservation constraints to them; similarly, in (17) for  $\rho \leftrightarrow \varrho$ . Whereas for small  $N_s$  the constraints cannot always be satisfied, for large enough Kraus rank, the quantum channel satisfies all the required constraints.

The problem of constructing an inverse quantum channel can be an attractive approach in certain ML/AI applications. It allows one to consider mappings from pure states to mixed states, a common setting in quantum information processing. In this case, the mapping becomes a quadratic function of the mapping operators, in the same way that the mapping (7) from a mixed state to a pure state yields a quadratic fidelity in the mapping operators for the direct quantum channel.

Our numerical experiments show that the inverted quantum channel provides similar properties to the direct one in terms of Choi matrix rank. A question arises: when can the inverse channel in ML applications be constructed simply by “swapping the indices”, besides for the unitary channel? If we drop the requirement of trace preservation, and require a single “simplified” condition (A2) – this allows the fidelity optimization problem to be reduced to an eigenvalue problem. The question of constructing alternative forms of constraints (not necessarily trace-preserving) that would allow for the direct construction of an inverse quantum channel is a subject of future research. In data analysis, other forms of constraints beyond trace preservation are often crucial.

### E. Reconstructing Projective Operators: Approaches and Applications

Besides constructing the inverse quantum channel (in this case, we typically have  $D = n$ , the unit matrix-to-unit matrix constraints (14) in the  $D < n$  case arise in the reconstruction of projections. Reconstructing projective operators is of particular interest in data analysis. Consider a space of dimension  $n$ , and a projective operator  $P$ , projecting it to a smaller subspace of dimension  $D$ .

Instead of the common condition  $P^2 = P$ , it is better to represent the unit matrix in the original space as

$$\mathbb{1} = \sum_{k=0}^{n-1} |\psi^{[k]}\rangle\langle\psi^{[k]}| \quad (30)$$

where  $\psi^{[k]}$  is an arbitrary orthogonal basis in the input vector space. Then we can select this basis as the direct sum of the desired subspace of dimension  $D$  and the orthogonal subspace, which has dimension  $n - D$ . From here, we immediately obtain that a projective operator is an operator that transforms a unit matrix of dimension  $n$  into a unit matrix of dimension  $D$ . That is, it is a Kraus rank-one ( $N_s = 1$ ) quantum channel with  $D < n$ , satisfying the constraints (14). This is a trace-decreasing map.

Assume we have a sample (6) with the mapping:

$$\psi^{(l)} \rightarrow \phi^{(l)} = \frac{|P|\psi^{(l)}\rangle}{\sqrt{\langle\psi^{(l)}|P^\dagger|P|\psi^{(l)}\rangle}} \quad (31)$$

where  $P$  is a projective operator. This means that  $\phi^{(l)}$  is a normalized projection of  $\psi^{(l)}$  onto some subspace. A trivial way of using the direct projections  $\langle\psi|\phi\rangle$  to reconstruct  $P$  is usually inapplicable, since random phases, similar to those in (25), are always assumed to exist in the measured data (these phases are  $\pm 1$  for real-valued data). The problem is reduced to maximizing the fidelity

$$\mathcal{F} = \sum_{l=1}^M \omega^{(l)} \frac{|\langle\phi^{(l)}|\mathcal{U}|\psi^{(l)}\rangle|^2}{\langle\psi^{(l)}|\mathcal{U}^\dagger|\mathcal{U}|\psi^{(l)}\rangle} \xrightarrow{\mathcal{U}} \max \quad (32)$$

for partially unitary operators  $\mathcal{U}$  with  $D < n$  that satisfy the constraints (14). These constraints are quadratic in  $\mathcal{U}$  and are perfectly applicable to the framework of this paper. However, the fidelity in (32) cannot be exactly reduced to the quadratic form (12), since for each  $l$ , there is an  $\mathcal{U}$ -dependent term in the denominator.

One can formally approximate (32) not by summing the individual terms, but instead by summing the numerator and denominator terms separately, and then considering their ratio:

$$\mathcal{F} \approx \frac{\sum_{l=1}^M \omega^{(l)} |\langle\phi^{(l)}|\mathcal{U}|\psi^{(l)}\rangle|^2}{\sum_{l=1}^M \nu^{(l)} \langle\psi^{(l)}|\mathcal{U}^\dagger|\mathcal{U}|\psi^{(l)}\rangle} \xrightarrow{\mathcal{U}} \max \quad (33)$$

where  $\nu^{(l)}$  are some weights. One may choose for example  $\nu^{(l)} = \omega^{(l)}$  and thus normalize (33) to the  $[0 : 1]$  interval. As discussed in [16], an important property required for any approximated fidelity is that it should attain its maximum when the mapping operators correspond to the sought quantum channel. For counterexamples, see Table I of [16]. Our numerical experiments show that the fidelity in (33) does not exhibit this issue when choosing  $\nu^{(l)} = \omega^{(l)}$ . The maximum of the fidelity corresponds

to the projective operator used to construct the sample, i.e., the projective operator is recovered exactly from the sample in (31).

This approximate expression represents the total fidelity as the ratio of two quadratic forms in the mapping operators. Whereas the total fidelity forms we previously considered were always a weighted sum of individual state matches (9), the total fidelity in the form of (33) differs from all of these: it aggregates the numerator and denominator separately and then considers their ratio. Numerical experiments show that this form of fidelity allows for the exact reconstruction of the projective operator. This is a critically important feature. See Table I of [16], where we demonstrated that for many fidelity approximations, their maximum is not reached for the channel used to create the mapping. For a quantum channel with  $N_s \geq 1$ , this form of the fidelity becomes:

$$\mathcal{F} = \frac{\sum_{s=0}^{N_s-1} \sum_{j,j'=0}^{D-1} \sum_{k,k'=0}^{n-1} B_{jk;s}^* S_{jk;j'k'} B_{j'k';s}}{\sum_{s=0}^{N_s-1} \sum_{j,j'=0}^{D-1} \sum_{k,k'=0}^{n-1} B_{jk;s}^* Q_{jk;j'k'} B_{j'k';s}} \xrightarrow{B} \max \quad (34)$$

where  $S_{jk;j'k'}$  is the familiar tensor from (11) and  $Q_{jk;j'k'}$  is a similar tensor obtained in the same way from the denominator of (33)

$$Q_{jk;j'k'} = \delta_{jj'} \sum_{l=1}^M \nu^{(l)} \psi_k^{(l)*} \psi_{k'}^{(l)} \quad (35)$$

Note that even if the basis  $\psi_k$  is chosen such that  $\delta_{kk'} = \langle \psi_k | \psi_{k'} \rangle$  holds for the actual relation, the sum in (35) is not equal to  $\delta_{kk'}$ . This sum is over the sample of input vectors in (31); this sample typically consists of a number of unrelated observations (e.g., a collection of images) mapped to some of its features (e.g., image content property). The sum  $\sum_{l=1}^M \nu^{(l)} \psi_k^{(l)*} \psi_{k'}^{(l)}$  characterizes the learning sample, not the relationship between  $\psi$  and  $\phi$ . In this sense, the tensor  $S_{jk;j'k'}$  (11) contains both: the information about the learning sample and the relation (31) that we want to learn. We discussed above the necessity for the initial conversion of the learning sample to a form that can be treated as a wavefunction mapping. Equation (5) is the simplest such form.

The expression in (34) is likely the most general form of the fidelity to which our theory can be applied. Whereas most of the existing works use a fidelity (such as in (27)) between individual states and then derive the total fidelity of a sample (such as the sample (7) with fidelity (9)), the form in (34) defines the total fidelity directly, without the intermediate step of state matching. Numerical experiments show that this form allows for the exact reconstruction of projective operators from the pure state mapping data sample (31).

The algorithm from Appendix A is directly applicable (at least in the  $N_s = 1$  case of finding regular projective operators) by replacing the simplified constraint in (A2) with the denominator of (34), e.g. as in Eq. (A15).

The problem can also be reduced to an SDP optimization problem by applying the approach from Appendix A to handle the diagonal elements of (14) for the operators  $B_{jk;s}$ , which satisfy the unit matrix-to-unit matrix constraints: replace the  $D$  diagonal elements in the inhomogeneous constraints with  $D - 1$  homogeneous constraints of the form  $G_{jj'} - G_{j-1,j'-1} = 0$ , and instead of requiring the sum of all diagonal elements to be equal to  $D$ , require the denominator of (34) to be equal to a constant. The idea is simple: replace the  $D$  diagonal elements in the inhomogeneous constraints with  $D - 1$  homogeneous constraints and a single inhomogeneous one, which then can be set to an arbitrary normalizing constant (note that (34) does not change when scaling  $B \rightarrow \text{const} \cdot B$ ).

$$\text{const} = \sum_{s=0}^{N_s-1} \sum_{j,j'=0}^{D-1} \sum_{k,k'=0}^{n-1} B_{jk;s}^* Q_{jk;j'k'} B_{j'k';s} \quad (36)$$

Equation (36) now replaces the simplified constraint (A2). The full set of constraints in (14) is now converted to (36) along with the remaining  $D(D + 1)/2 - 1$  homogeneous constraints. These constraints are then used to construct the  $A_c$  matrices in (23).

We conducted numerical testing for projective operator reconstruction in a manner similar to unitary learning in Section IV A. A projective operator  $P$  was created by taking the first  $D$  rows from a unitary operator generated from random data. Then, for randomly generated  $\psi^{(l)}$ , we applied the operator  $P$  and normalized the result to the state  $\phi^{(l)}$  (31). This follows a typical form of the data in ML and AI: normalized vectors of different dimensions. Next, the tensors  $S_{jk;j'k'}$  and  $Q_{jk;j'k'}$  were created, and the corresponding optimization problem with the fidelity in (33) was solved. In all cases, the solution was the Choi matrix of rank one, and we selected the corresponding eigenvector. It matched exactly the projective operator  $P$  that was used to generate the sample. Both CVXPY and SDPA were able to find the solution, and it always matched the original operator  $P$ . If we were to plot the fidelity and rank for a fixed  $n$  and varied  $1 \leq D \leq n$ , it would resemble the exact reconstruction for unitary learning shown in Fig. 1: rank one and fidelity equal to one. This contrasts with the difficulties discussed in [15], Section V, where using a fidelity of a form other than (34) produced artifacts in the reconstruction for  $D < n$ , while no artifacts were observed for unitary learning with  $D = n$ . See the class `com/polytechnik/sdpexternalsolvers/TestChoiMatrixProjections.java`, which demonstrates the reconstruction of projective operator from the sample in (31) using the fidelity (33).

A natural extension of projective operators is a higher-rank Kraus CP quantum channel, which converts a unit matrix to a unit matrix, i.e., the constraints (14) with  $N_s > 1$ . In ML/AI, the IN/OUT data is typically normalized to 1, similar to (31) for projective operators. In this case, the fidelity in (34) allows for the reconstruction of “projective-type” quantum channels. This form of knowledge representation can be highly advantageous for

ML.

In this section, we demonstrate the application of the theory to reconstruct projective operators from data. This is possible if we approximate the fidelity as a ratio of two quadratic forms in the mapping operators, as shown in (34). This is likely the most general form of the fidelity to which our theory can be applied. This represents an important generalization of the quadratic fidelity in mapping operators (12) that we previously considered. The fidelity form in (34) enables the construction of a much broader variety of proxy fidelities (approximations). In our previous work [16], when the proper fidelity in the form of (12) could not be constructed, we used approximations in the same form (12) and highlighted the limitations of such approximations. The newly suggested form in (34) significantly expands the range of possible approximations that can be used, facilitating the reconstruction of quantum channels of various forms from a broader set of sample data.

## V. CONCLUSION

In this work we demonstrated that, when the fidelity is a ratio of two quadratic function in mapping operators, a powerful SDP technique can be applied to reconstruct the quantum channel from data. Commercial SDP optimization software is directly applicable to problems with Choi matrix dimensions under  $1000 \times 1000$ . The optimization problem typically results in a low-rank Choi matrix, typically under a few percent of the matrix dimension. This low Kraus rank property has deep significance in AI and ML applications: a relatively small Kraus rank quantum channel is typically sufficient to describe experimentally observed data.

A quantum channel learning representation can be considered a natural extension of unitary learning[12–14]; the convex nature of the optimization problem makes this approach especially appealing for practical applications.

This work considers the reconstruction of a single quantum channel from classical mapping data. The mapping itself can be seen as a form of computation. A quantum computation algorithm consists of a sequence of unitary transformations. For a given initial state, the quantum system’s unitary evolution produces the desired computational result. In ML/AI, unitary learning is typically used differently: the input state is transformed into an output, and the specific components of the output state are considered the features of interest that the ML system predicts. Contrary to quantum computations, where simple gates are used (as it is assumed that simpler gates are easier to implement in a physical system), these classical unitary mappings are not necessarily required to be simple. The quantum channel transformation (1) can be considered a form of computation, one way or another.

In this work, the reconstruction of a single quantum channel (2) from IN/OUT classical data has been considered. In [17], we introduced the hierarchical concept of a

density matrix network, where a large quantum channel is represented as hierarchical transformations by simpler quantum channels. Similar to how perceptron weights, combined with an activation function, create specialized components that are then combined into a neural network, we can consider a hierarchical quantum channel in a similar way.

Importantly, since the SDP problem is convex, the optimization of the total quantum channel can be performed as an iteration over individual, much smaller components. This “incremental learning” feature is seldom in neural networks, it is typically available only for specific topologies. Since the SDP problem for quantum channels is convex, this incremental learning feature is available for an arbitrary quantum channel. The specific topology chosen for the density matrix network is simply a matter of computational optimization. For smaller dimensions, the problem can always be optimized directly without assuming any particular topology, using the SDP technique we considered in this paper. This contrasts with neural networks, where selecting the proper topology is a crucial factor for success. We believe that representing knowledge in the form of a quantum channel allows for modeling a wide variety of data types. The observed low rank of the reconstructed Choi matrix leads us to conclude that low Kraus rank quantum channels are typically sufficient to map classical data. It is important to note that the developed approach can also be applied to other forms of quantum channels, such as projective operators.

## ACKNOWLEDGMENTS

This research was supported by Autretech Group, a resident company of the Skolkovo Technopark. We thank our colleagues from the Autretech R&D department who provided insight and expertise that greatly assisted the research. Our grateful thanks are also extended to Mr. Gennady Belov for his methodological support in doing the data analysis.

Vladislav Malyshkin is grateful to Yaroslav Mikhailovich Beltukov for stimulating discussions on the applications of Semidefinite Programming to physical problems, and to Eugenius Levovich Ivchenko for his comments regarding the requirement of a simple demonstration of the technique, which is now addressed in Section IV A.

The article was written based on the presentation at the colloquium on the occasion of the 96th anniversary of Iya Pavlovna Ipatova’s[38] birthday, held on December 19, 2025.

## Appendix A: Quantum Channel Representation in Lower Diagonal Matrix Form

The optimization problem we consider is to maximize the total fidelity (12) over the space of Kraus operators  $B_s$

(1), subject to the constraints (13) or (14). The main idea behind our algebraic technique for numerical computations is to replace the quadratic constraints (13) or (14) with a single simplified (partial) quadratic constraint, which is typically the sum of the diagonal elements, and a set of convergence-helper homogeneous linear constraints derived from the remaining quadratic constraints. This allows us to employ the eigenvalue problem as the main iterative step, with the convergence-helper constraints reducing the size of the vector space. For unitary mapping, vectorizing the unitary operator provides a proper parametrization of the search space. The problem is non-convex, but multiple solution candidates (eigenvectors) greatly increase the chances of finding the global maximum compared to methods based on gradient- or Newton-type algorithms, which generate only a single solution candidate.

For a quantum channel (1), a similar approach was developed in [16]. There, we considered the quantum channel in its canonical representation,  $\text{Tr}B_s B_{s'}^\dagger \sim \delta_{ss'}$ . This required an additional  $N_s(N_s - 1)/2$  constraints and corresponding Lagrange multipliers. The updated version of the algorithm presented below uses the Cholesky decomposition to eliminate these extra constraints. Now, a requirement for some components of the  $B_s$  matrix to be zero arises explicitly, which allows for the elimination of the extra constraints, thus avoiding an increase in the search space and the need for additional Lagrange multipliers. The idea is to parametrize  $\mathcal{J}$  (16) as a product of two matrices

$$\mathcal{J} = B^* B^T \quad (\text{A1})$$

where  $B_{jk;s}$  is now a lower-diagonal matrix of dimension  $Dn \times N_s$ . This form is actually Eq. (16), with the “gauge” for  $B_{jk;s}$  being a lower-diagonal matrix. By choosing  $N_s$ , we can construct a quantum channel of any required Kraus rank  $N_s$ . The matrix elements  $B_{jk;s}$  are nonzero only for  $s \leq jn + k$  with  $s < N_s$ . From a computational perspective, an important property is that the full trace  $\text{Tr}B^* B^T$  reduces to a simple Frobenius norm:

$$|B|^2 = \sum_{s=0}^{N_s-1} \sum_{j=0}^{D-1} \sum_{k=0}^{n-1} |B_{jk;s}|^2 \quad (\text{A2})$$

This gives a vector-style  $L^2$  norm for the operator  $B$ . When all elements of  $B$  are stored consecutively in a single vector (row by row), the full-trace operation becomes ordinary vector scalar products.

$$\langle B | \check{B} \rangle = \text{Tr}B^* \check{B}^T = \sum_{s=0}^{N_s-1} \sum_{j=0}^{D-1} \sum_{k=0}^{n-1} B_{jk;s}^* \check{B}_{jk;s} \quad (\text{A3})$$

This  $LL^T$  (Cholesky-type) decomposition is often used to parametrize positive semidefinite matrices. Whereas the problem in the form (22) subject to (23) and CP constraints (21) is a convex SDP optimization problem [21], the  $LL^T$  transformation automatically satisfies only the CP constraints. The actual problem written in this new

basis may not always retain the convexity property. In some cases, a convexity-like behavior may still be observed, and an arbitrary optimization method can effectively find the solution to the convex optimization problem. In our case, we used eigenvalue-based optimization, which is not particularly sensitive to problem convexity. For any individual problem, the convexity property in the  $LL^T$  basis should be initially checked to decide on the appropriate optimization method to apply.

In the form (A1) with  $N_s \leq Dn$ , this representation allows us to efficiently parametrize  $\mathcal{J}$  for any desired Kraus rank  $N_s$ . Unitary learning corresponds to  $N_s = 1$ , with the sought operator  $\mathcal{U}$  stored in a single column. A quantum channel of Kraus rank three corresponds to a lower diagonal  $B$  matrix with  $Dn$  rows and  $N_s = 3$  columns of lengths  $Dn$ ,  $Dn - 1$ , and  $Dn - 2$ , respectively.

$$B = \begin{pmatrix} * & 0 & 0 & 0 & \dots & 0 \\ * & * & 0 & 0 & \dots & 0 \\ * & * & * & 0 & \dots & 0 \\ * & * & * & 0 & \dots & 0 \\ \vdots & \vdots & \vdots & \vdots & & \vdots \\ * & * & * & 0 & \dots & 0 \end{pmatrix} \quad (\text{A4})$$

From a computational viewpoint, an eigenproblem (obtained using the simplified, partial constraint) in the space of operators  $B$  becomes an ordinary eigenproblem for a vector of dimension  $DnN_s - N_s(N_s - 1)/2$ , i.e.,

$$\dim = \frac{(2Dn - N_s + 1)N_s}{2} \quad (\text{A5})$$

which is the number of non-zero elements in (A4). The major difference from the SDP problem discussed above – which always assumes  $N_s = Dn$  – is that here we can construct a solution with a pre-specified Kraus rank  $N_s$ . Imposing a specific rank on  $\mathcal{J}$  in addition to the PSD condition  $\mathcal{J} \succeq 0$  (21) makes the problem non-convex and significantly more difficult.

Importantly, from the perspective of numerical implementation, that the representation (A1) creates a problem very similar to the one we previously considered. The only difference from the algorithm in [15] lies in the increased dimension of the eigenproblem, which becomes (A6) for constraint (13) and (A7) for constraint (14) when the convergence-helper linear constraints are taken into account.

$$\dim_{\text{Tr}} = \frac{(2Dn - N_s + 1)N_s}{2} - \frac{n(n+1)}{2} + 1 \quad (\text{A6})$$

$$\dim_{\mathbb{1}} = \frac{(2Dn - N_s + 1)N_s}{2} - \frac{D(D+1)}{2} + 1 \quad (\text{A7})$$

This illustrates the main strengths and weaknesses of the approach. Whereas for unitary learning ( $D = n$ ,  $N_s = 1$ ) the eigenproblem dimension grows as  $O(n^2)$ , for a full-rank quantum channel ( $N_s = Dn$ ) the eigenproblem dimension grows as  $O(n^4)$  when  $D = n$ . However, as

discussed in Section III, the latter problem is convex and can be solved using other optimization methods. The case of a low-Kraus-rank quantum channel (low  $N_s$ ) is more difficult and represents the main application problem for the algorithm we developed in [15].

The optimization problem consists in Lagrangian optimization. In this appendix, we consider the unit input matrix to unit output matrix constraint (14),

$$G_{jj'}(B, \check{B}) = \sum_{s=0}^{N_s-1} \sum_{k=0}^{n-1} B_{jk;s}^* \check{B}_{j'k;s} \quad (\text{A8})$$

$$\delta_{jj'} = G_{jj'}(B, B) \quad (\text{A9})$$

for the solution  $B_{jk;s}$  (A4) as it is somewhat easier to handle numerically. The constraints are analogous to (A3), but now the partial trace is used in (A8). The formulas corresponding to the trace preservation constraints (13) are presented in Appendix A 1 below. Introduce a Lagrangian.

$$\begin{aligned} \mathcal{L} = & \sum_{s=0}^{N_s-1} \sum_{j,j'=0}^{D-1} \sum_{k,k'=0}^{n-1} B_{jk;s}^* S_{jk;j'k'} B_{j'k';s} \quad (\text{A10}) \\ & + \sum_{j,j'=0}^{D-1} \lambda_{jj'} \left[ \delta_{jj'} - \sum_{s=0}^{N_s-1} \sum_{k'=0}^{n-1} B_{jk';s}^* B_{j'k';s} \right] \end{aligned}$$

Note that in (12), the tensor  $S_{jk;j'k'}$  appears exactly the same for all  $s$  and for all Kraus operators  $B_s$ . This leads to degeneracy in the optimization problem. However, if instead of general  $B$  we use lower lower diagonal  $B_{jk;s}$  from (A4), this degeneracy does not occur, because for each fixed  $s$  the corresponding vector  $B_{jk;s}$  contains a different number of non-zero elements (indexed by the scalar index  $jn + k$ , corresponding to a row in (A4) and column  $s$ ). While the first term in (A10) may appear similar to (12), it is in fact different, because it eliminates the upper-diagonal terms in  $B_{jk;s}$  (A4). In (A10), one may think of  $S_{jk;j'k'}$  as effectively depending on  $s$  through the condition  $s \leq \min(jn + k, N_s - 1)$ , i.e., as  $S_{s,jk;s',j'k'}$ , which is necessary to avoid the degeneracy of the problem discussed in [16]. This is an important feature of the Cholesky decomposition (A1).

In the  $N_s = 1$  case, varying (A10) yields the familiar Lagrange stationarity condition, which results in the algebraic problem introduced in [15]:

$$S\mathcal{U} = \lambda\mathcal{U} \quad (\text{A11})$$

In the  $N_s > 1$  case a similar algebraic problem with respect to lower diagonal  $B$  can be obtained, but it's analysis requires a separate study.

An important idea of the numerical method is the introduction of a simplified (partial) constraint, which is the sum of all diagonal elements of (A8); this yields (A2) with  $|B|^2 = D$ . To obtain the optimization problem when using simplified (partial) constraints instead of the proper ones, the variation of  $\mathcal{L}$  gives the eigenvectors of the matrix

$$\mathcal{S}_{jk;j'k'}$$

$$\mathcal{S}_{jk;j'k'} = S_{jk;j'k'} - \lambda_{jj'} \delta_{kk'} \quad (\text{A12})$$

$$\frac{\sum_{s=0}^{N_s-1} \sum_{j,j'=0}^{D-1} \sum_{k,k'=0}^{n-1} B_{jk;s}^* \mathcal{S}_{jk;j'k'} B_{j'k';s}}{\sum_{s=0}^{N_s-1} \sum_{j=0}^{D-1} \sum_{k=0}^{n-1} |B_{jk;s}|^2} \xrightarrow{B} \max \quad (\text{A13})$$

$$\sum_{j,j'=0}^{D-1} \sum_{k,k'=0}^{n-1} \mathcal{S}_{jk;j'k'} B_{j'k';s}^{[i]} = \mu^{[i]} B_{jk;s}^{[i]} \quad (\text{A14})$$

The problem (A14) is an eigenproblem of dimension (A5), since only the non-zero terms with  $s \leq \min(jn + k, N_s - 1)$  are retained. For numerical implementation, one can think of  $B_{jk;s}$  as a vector  $B_i$  of length (A5), where the scalarized multi-index  $i$  ranges from 0 to  $\dim - 1$ .

As discussed in Section IV E, for reconstructing projective operators, the fidelity in (34) can be expressed in the form where, instead of using the simplified constraint (A2), one may use the denominator in (34). This leads to a slight modification in the formulas, with the Lagrangian

$$\begin{aligned} \mathcal{L} = & \frac{\sum_{s=0}^{N_s-1} \sum_{j,j'=0}^{D-1} \sum_{k,k'=0}^{n-1} B_{jk;s}^* S_{jk;j'k'} B_{j'k';s}}{\sum_{s=0}^{N_s-1} \sum_{j,j'=0}^{D-1} \sum_{k,k'=0}^{n-1} B_{jk;s}^* Q_{jk;j'k'} B_{j'k';s}} \quad (\text{A15}) \\ & + \sum_{j,j'=0}^{D-1} \lambda_{jj'} \left[ \delta_{jj'} - \sum_{s=0}^{N_s-1} \sum_{k'=0}^{n-1} B_{jk';s}^* B_{j'k';s} \right] \end{aligned}$$

instead of (A10). This form results in a generalized eigenproblem similar to (A14), but with the  $Q_{jk;j'k'}$  tensor appearing on the right-hand side. The formula for the Lagrange multipliers  $\lambda_{jj'}$ , as given in (A19), is also slightly modified to include  $Q_{jk;j'k'}$ .

As discussed in [15, 16], the direct optimization of (A13), which leads to an eigenproblem of dimension (A5), does not guarantee algorithm convergence. To reduce the basis dimension to (A7) and achieve convergence, it is necessary to include convergence-helper homogeneous linear constraints derived from the quadratic constraints (A9). See Appendix A.5 of [16] for the formulas and `com/polyte chnik/kgo/LLTbasis.java:getHelperConstraintsOf fdiag0DiagEq` for an updated numerical implementation. The idea is simple: for a given solution candidate  $B$ , find  $D(D+1)/2 - 1$  constraints  $C^{(m)}$  such that, for an arbitrary  $\check{B}$ ,  $D(D-1)/2$  of them will have  $\langle C^{(m)} | \check{B} \rangle$  from (A3) equal to the sum of two off-diagonal ( $j_m \neq j'_m$ ) elements  $G_{j_m j'_m}(B, \check{B}) + G_{j'_m j_m}^*(B, \check{B})$  from (A8), and  $D-1$  of them will have  $\langle C^{(m)} | \check{B} \rangle$  equal to the difference of two diagonal elements:  $G_{j_m j_m}(B, \check{B}) - G_{j_{m-1} j_{m-1}}(B, \check{B})$ .

After this, at the eigenvalue-selection step of the reduced-size (A7) eigenproblem, one needs to choose the eigenvector  $B_{jk;s}^{[i]}$  corresponding to the maximal eigenvalue. Numerical experiments show that this choice leads

to convergence to the global maximum, especially in the unitary case.

The obtained solution  $B_{jk;s}$  may not satisfy the full set of constraints (A9); only the partial constraint (A2) is always satisfied. To adjust the solution, we apply the  $G^{-1/2}$  transform (see Ref. [16], Eq. (A23)), which then yields the fully constrained solution:

$$\tilde{B}_{jk;s} = \sum_{j'=0}^{D-1} G_{jj'}^{-1/2} B_{j'k;s} \quad (\text{A16})$$

Here  $G_{jj'}^{-1/2}$  denotes the inverse square root of the Gram matrix (A8), calculated at the current iteration  $B_{jk;s}$ . If the Gram matrix has a zero eigenvalue, the adjustment procedure will fail. For some combinations of  $N_s, D, n$ , the constraints cannot be satisfied for an arbitrary  $B$ . For example, when  $N_s = 1$  and  $D < n$  in the case of the trace-preserving constraints (13), the matrix  $G$  (A23) has at least  $n - D$  zero eigenvalues. We should also note that applying  $G_{jj'}^{-1/2}$  (A16) could potentially cause  $\tilde{B}_{jk;s}$  to no longer belong to the set of lower diagonal matrices (A4). This issue is technical and can be readily resolved. The proposed transform allows for the conversion of an arbitrary quantum channel  $B_{jk;s}$  (1) to an entirely equivalent form of lower-diagonal matrices (A4). For a similar transformation to canonical form, see Appendix A.1 of Ref. [16]. Note that in (A1), one can write it as

$$\mathcal{J} = B^* Q Q^\dagger B^T \quad (\text{A17})$$

where  $Q$  is an arbitrary unitary operator of dimension  $N_s$ . Expanding the upper  $N_s$  rows of  $\tilde{B}_{jk;s}$ , which form a matrix  $M_{jk;s}$  of dimension  $N_s \times N_s$ , using the **QR decomposition**, we obtain (for real space):

$$M^T = QR \quad (\text{A18})$$

where  $Q$  is the orthogonal matrix and  $R$  is the upper diagonal matrix. From here, it follows that the matrix  $Q$  will transform  $\tilde{B}_{jk;s}$  into the lower diagonal form of (A4). See the class `com/polytechnik/kgo/LLTbasis.java:ConvertStateToLowerDiagMatrix`, which uses QR decomposition to obtain  $B$  in the lower diagonal form that can be used as a vector. This transform is an identity and does not change  $\mathcal{J}$  (A17).

The final step of the iteration is to update the Lagrange multipliers matrix  $\lambda_{ji}$ . Following [17], we obtain the expression:

$$\lambda_{ji} = \text{Herm} \sum_{s=0}^{N_s-1} \sum_{j'=0}^{D-1} \sum_{k,k'=0}^{n-1} B_{ik;s}^* S_{jk;j'k'} B_{j'k';s} \quad (\text{A19})$$

which can also be obtained directly by multiplying  $\frac{\delta \mathcal{L}}{\delta B_{jk;s}^*}$  by  $B_{ik;s}^*$  and summing over  $s$  and  $k$ , without considering a dual problem. The expression (A19) generalizes the standard eigenvalue relation  $\lambda = \langle \psi | H | \psi \rangle$ .

The current version of the algorithm differs from the algorithm in Ref. [16] in only one significant respect: it

now uses the Cholesky decomposition (A1) to represent the state. This allows us, in the  $N_s > 1$  case, to eliminate problem degeneracy and to require only a *single* solution adjustment (A16). The updated version uses  $N_s(N_s - 1)/2$  fewer variables than the version described in [16]; therefore, no “second set” of Lagrange multipliers  $\nu_{ss'}$  is required, as in Eq. (A2) of Ref. [16]. As long as we seek only the global solution of the optimization problem (A10) (that is, no “external” linear constraints are used, which would be required to build a hierarchy of solutions), only a single solution adjustment (A16) is applied, thereby avoiding two potentially conflicting transformations. In the  $N_s = 1$  case, the described algorithm is identical to that in [15].

## 1. Trace-Preserving Constraints: Mathematical Formulations and Equations

The most commonly considered constraint for a quantum channel map (1) is trace preservation (13). This is an alternative to (14), which enforces the constraint that the unit matrix  $A^{IN}$  is mapped to the unit matrix  $A^{OUT}$ . The technical meaning of this constraint is to construct a unit matrix of dimension  $n \times n$  from a sum of  $N_s$  matrices of the same dimension, each with rank  $D$  (or lower). For a unitary mapping with  $N_s = 1$  and  $D = n$ , both forms of constraints coincide. For the trace-preservation constraints (13), the following modifications apply.

Instead of (A10), the Lagrangian corresponding to the trace preservation constraints (19) is

$$\mathcal{L} = \sum_{s=0}^{N_s-1} \sum_{j,j'=0}^{D-1} \sum_{k,k'=0}^{n-1} B_{jk;s}^* S_{jk;j'k'} B_{j'k';s} + \sum_{k,k'=0}^{n-1} \lambda_{kk'} \left[ \delta_{kk'} - \sum_{s=0}^{N_s-1} \sum_{j'=0}^{D-1} B_{j'k;s}^* B_{j'k';s} \right] \quad (\text{A20})$$

In the  $N_s = 1$  case, varying (A20) yields the familiar Lagrange stationarity condition, which results in the algebraic problem:

$$S\mathcal{U} = \mathcal{U}\lambda \quad (\text{A21})$$

Instead of (A12), the variation of  $\mathcal{L}$  (A20) yields a matrix from which the solution candidates can be obtained as its eigenvectors:

$$S_{jk;j'k'} = S_{jk;j'k'} - \lambda_{kk'} \delta_{jj'} \quad (\text{A22})$$

Instead of (A16) the solution adjustment transform now is:

$$G_{kk'} = \sum_{s=0}^{N_s-1} \sum_{j=0}^{D-1} B_{jk;s}^* B_{jk';s} \quad (\text{A23})$$

$$\tilde{B}_{jk;s} = \sum_{k'=0}^{n-1} G_{kk'}^{-1/2} B_{jk';s} \quad (\text{A24})$$

When the Kraus rank  $N_s$  is insufficient, the Gram matrix (A23) may have zero eigenvalues, and the transform (A24) cannot be applied. In practice, the matrix (A23) is more likely to have a zero eigenvalue than the matrix (A8) that we considered above. Also, similarly to the above, the obtained  $\tilde{B}_{jk;s}$  may not satisfy the lower diagonal condition (A4). This issue can be resolved in the same way using the QR transform (A18).

Instead of (A19), the expression for the Lagrange multipliers for the next iteration is:

$$\lambda_{kq} = \text{Herm} \sum_{s=0}^{N_s-1} \sum_{j,j'=0}^{D-1} \sum_{k'=0}^{n-1} B_{jq;s}^* S_{jk;j'k'} B_{j'k';s} \quad (\text{A25})$$

Everything else regarding the trace-preservation constraints (13) is almost identical to the expressions presented above in Appendix A for the constraints (14).

## 2. Numerical Implementation Approach and Challenges

For the updated version of this algorithm, see the class `com/polytechnik/kgo/QCInverseProblem.java`, which implements the algorithm of above. Compared to the older version, `com/polytechnik/kgo/KGOIterationalSubspaceLinearConstraintsB.java`, it removes all the “external” constraints code (used to build a hierarchy of solutions) and explicitly takes the value of the Kraus rank  $N_s$  as an argument. For  $N_s = 1$ , it is almost identical to `com/polytechnik/kgo/KGOIterationalSubspaceLinearConstraintsB.java` from [16] and `com/polytechnik/kgo/KGOIterationalSubspaceLinearConstraints.java` from [15], with external constraints disabled. Also, see the class `com/polytechnik/kgo/LLTbasis.java`, which now includes all operations in the lower diagonal basis of the Cholesky decomposition (A1). The introduction of this class makes the implementation in `com/polytechnik/kgo/QCInverseProblem.java` much cleaner. Additionally, this class is used to create the matrices  $A_c$  (23) when using commercial SDP software.

Whereas the physical applications are demonstrated and discussed in Section IV above, this appendix focuses only on the numerical aspects of the developed algorithm. What allows the algorithm to find the global maximum is its use of the eigenproblem (A13) as the core building block. While derivative-based methods do not guarantee finding the global maximum, the use of the eigenproblem guarantees finding the globally optimal solution in the space of dimension  $\dim_{\text{Tr}}$  (A6) for the constraints (13) or  $\dim_1$  (A7) for the constraints (14). What prevents the algorithm from finding the global maximum in a single step and requires iterations is the fact that the space in which we search for the solution is known only approximately. Therefore, iterations are required. This space is determined by the convergence-helper homogeneous linear constraints derived from the quadratic constraints (13) or (14). For a real-valued space, there are

$n(n+1)/2 - 1$  and  $D(D+1)/2 - 1$  constraints, respectively. Numerical experiments show the crucial importance of the convergence-helper constraints; removing even a single one often prevents the algorithm from converging.

The numerical testing of the algorithm from Appendix A demonstrates its ability to reconstruct a quantum channel for relatively low values of  $N_s$ . For  $N_s \gtrsim 4$ , the algorithm often iterates near Kraus rank-one solutions, and it frequently takes a large number of iterations to escape from a Kraus rank-one local maximum. The selection of the state corresponding to a non-maximal eigenvalue at iteration step can improve the situation to some extent.

There is an important synergy between the described algorithm and SDP programming. For the quantum channel reconstruction problem, satisfaction of the constraints (19) or (20) can be readily obtained from the current iteration Choi matrix  $\mathcal{J}_{jk;j'k'}$  (16). First, the matrix  $G_{kk'}$  (A23) or  $G_{jj'}$  (A8) can be obtained as a partial trace of the current Choi matrix  $\mathcal{J}_{jk;j'k'}$ . Then, by applying the transformation

$$\tilde{\mathcal{J}}_{jk;j'k'} = \sum_{k'',k'''=0}^{n-1} G_{kk''}^{-1/2} G_{k'k''}^{-1/2} \mathcal{J}_{jk'';j'k''} \quad (\text{A26})$$

$$\tilde{\mathcal{J}}_{jk;j'k'} = \sum_{j'',j'''=0}^{D-1} G_{jj''}^{-1/2} G_{j'j''}^{-1/2} \mathcal{J}_{j''k;j'''k'} \quad (\text{A27})$$

one can immediately obtain the Choi matrix satisfying the constraints (19) or (20), respectively. This transformation creates a “minimal disturbance” to the current iteration of  $\mathcal{J}_{jk;j'k'}$  and allows for an efficient optimization of the SDP algorithm.

## Appendix B: Software Usage Description

The software [39] is written in Java. The related code is in the `com/polytechnik/{kgo,utils,sdpexternalsolvers}` directories. To test the provided software, install Java 25 or later, install CVXPY[35] as `pip3 install cvxpy`, and recompile and install SDPA[33] from `sdpa.sourceforge.net`. Additionally install the Gson library from `github.com/google/gson`.

Download the source code [39] from the archive `AMuseOfCashFlowAndLiquidityDeficit.zip`, then decompress and recompile it. Here, we use the backslash “\” to split lines to fit the two-column PRE format; BASH interprets it correctly, allowing the commands to be copied directly from the article into the BASH prompt.

```
unzip AMuseOfCashFlowAndLiquidityDeficit.zip
javac -g com/polytechnik/\
{kgo,utils,sdpexternalsolvers}/*java
```

Create a JNI library `com/polytechnik/sdpexternalsolvers/libSDPAsolver.so` linking to SDPA. Run the linking commands from the `com/polytechnik/sdpexternalsolvers/SDPAsolver.java` javadoc section. After that one can run the provided software:

```
java -Djava.library.path=\
com/polytechnik/sdpexternalsolvers/ \
com/polytechnik/sdpexternalsolvers/\
TestChoiMatrixUnitaryLearning
```

See other programs in the classes `com/polytechnik/sdp`

`externalsolvers/{TestChoiMatrixProjections, Tes  
tChoiMatrixUnitaryLearning, TestChoiMatrixRank0  
nRandomSK, TestChoiMatrixRankOnSKFromRandomSamp  
le, TestChoiMatrixRankOnSKFromQuantumChannelOut  
PureAsMaxEVofRho}.java`. Test usage is provided in the  
javadoc preamble.

---

[1] V. Vapnik and A. Y. Chervonenkis, The method of ordered risk minimization, I, *Avtomatika i Telemekhanika* **8**, 21 (1974).

[2] P. Hájek and T. Havránek, On generation of inductive hypotheses, *International Journal of Man-Machine Studies* **9**, 415 (1977).

[3] V. Vapnik, *The nature of statistical learning theory* (Springer science & business media, 2013).

[4] I. H. Witten and E. Frank, Data mining: practical machine learning tools and techniques with Java implementations, *Acm Sigmod Record* **31**, 76 (2002).

[5] L. A. Zadeh, Fuzzy sets, *Information and control* **8**, 338 (1965).

[6] P. Hájek, Fuzzy logic and arithmetical hierarchy, *Fuzzy sets and Systems* **73**, 359 (1995).

[7] Y. Bengio, A. Courville, and P. Vincent, Representation learning: A review and new perspectives, *IEEE transactions on pattern analysis and machine intelligence* **35**, 1798 (2013).

[8] A. Jamiołkowski, Linear transformations which preserve trace and positive semidefiniteness of operators, *Reports on mathematical physics* **3**, 275 (1972).

[9] M.-D. Choi, Completely positive linear maps on complex matrices, *Linear algebra and its applications* **10**, 285 (1975).

[10] K. Kraus, *States, Effects, and Operations: Fundamental Notions of Quantum Theory*, Lecture Notes in Physics, Vol. 190 (Springer-Verlag, 1983) Lectures in Mathematical Physics at the University of Texas at Austin.

[11] V. P. Belavkin and P. Staszewski, A Radon-Nikodym theorem for completely positive maps, *Reports on mathematical physics* **24**, 49 (1986).

[12] A. Bisio, G. Chiribella, G. M. D'Ariano, S. Facchini, and P. Perinotti, Optimal quantum learning of a unitary transformation, *Physical Review A* **81**, 032324 (2010).

[13] M. Arjovsky, A. Shah, and Y. Bengio, Unitary evolution recurrent neural networks, in *International conference on machine learning, NY, USA, 2016* (Proceedings of Machine Learning Research (proceedings.mlr.press), 2016) pp. 1120–1128.

[14] S. Hyland and G. Rätsch, Learning unitary operators with help from  $u(n)$ , in *Proceedings of the AAAI Conference on Artificial Intelligence*, Vol. 31 (Association for the Advancement of Artificial Intelligence (aaai.org), 2017).

[15] M. G. Belov and V. G. Malyshkin, Partially unitary learning, *Phys. Rev. E* **110**, 055306 (2024).

[16] M. G. Belov, V. V. Dubov, A. V. Filimonov, and V. G. Malyshkin, Quantum channel learning, *Phys. Rev. E* **111**, 015302 (2025).

[17] M. G. Belov, V. V. Dubov, V. K. Ivanov, A. Y. Maslov, O. V. Proshina, and V. G. Malyshkin, Superstate Quantum Mechanics, arXiv preprint arXiv:2502.00037 10.48550/arXiv.2502.00037 (2025).

[18] M. M. Wilde, Recoverability for Holevo's just-as-good fidelity, in *2018 IEEE International Symposium on Information Theory (ISIT)* (IEEE, 2018) pp. 2331–2335.

[19] A. A. Budini, R. L. de. M. Filho, and M. F. Santos, Quantum distinguishability measures: Projectors versus state maximization, *Physical Review A* **110**, 022228 (2024).

[20] N. Johnston and D. W. Kribs, Quantum gate fidelity in terms of Choi matrices, *Journal of Physics A: Mathematical and Theoretical* **44**, 495303 (2011).

[21] S. Boyd and L. Vandenberghe, *Convex optimization* (Cambridge university press, 2004).

[22] V. G. Malyshkin, On The Radon-Nikodym Spectral Approach With Optimal Clustering, arXiv preprint arXiv:1906.00460 10.48550/arXiv.1906.00460 (2019).

[23] M. G. Belov, V. V. Dubov, V. K. Ivanov, A. Y. Maslov, O. V. Proshina, and V. G. Malyshkin, Trade Execution Flow as the Underlying Source of Market Dynamics, arXiv preprint arXiv:2511.01471 10.48550/arXiv.2511.01471 (2025).

[24] M. M. Wilde, From classical to quantum Shannon theory, arXiv preprint arXiv:1106.1445 10.48550/arXiv.1106.1445 (2011).

[25] C. H. Baldwin, A. Kalev, and I. H. Deutsch, Quantum process tomography of unitary and near-unitary maps, *Physical Review A* **90**, 012110 (2014).

[26] M. Holzapfel, T. Baumgratz, M. Cramer, and M. B. Plenio, Scalable reconstruction of unitary processes and Hamiltonians, *Physical Review A* **91**, 042129 (2015).

[27] L. Vandenberghe and S. Boyd, Semidefinite programming, *SIAM review* **38**, 49 (1996).

[28] H. Wolkowicz, R. Saigal, and L. Vandenberghe, *Handbook of semidefinite programming: theory, algorithms, and applications*, Vol. 27 (Springer Science & Business Media, 2012).

[29] J.-B. Lasserre, *Moments, positive polynomials and their applications*, Vol. 1 (World Scientific, 2009).

[30] M. F. Anjos and J. B. Lasserre, *Handbook on semidefinite, conic and polynomial optimization*, Vol. 166 (Springer Science & Business Media, 2011).

[31] Z. Wen and W. Yin, A feasible method for optimization with orthogonality constraints, *Mathematical Programming* **142**, 397 (2013).

[32] P. Taranto, S. Milz, M. Murao, M. T. Quintino, and K. Modi, Higher-Order Quantum Operations, arXiv preprint arXiv:2503.09693 10.48550/arXiv.2503.09693 (2025).

[33] M. Yamashita, K. Fujisawa, K. Nakata, M. Nakata, M. Fukuda, K. Kobayashi, and K. Goto, A high-performance software package for semidefinite programs: SDPA 7, *Tokyo, Japan* (2010).

[34] M. Andersen, J. Dahl, and L. Vandenberghe, *CVXOPT: Python software for convex optimization*, <http://cvxopt.org/> (2015), version 1.7.

- [35] S. Diamond and S. Boyd, CVXPY: A Python-embedded modeling language for convex optimization, *Journal of Machine Learning Research* **17**, 1 (2016).
- [36] G. Torlai, C. J. Wood, A. Acharya, G. Carleo, J. Carrasquilla, and L. Aolita, Quantum process tomography with unsupervised learning and tensor networks, *Nature Communications* **14**, 2858 (2023).
- [37] M. A. Nielsen and I. L. Chuang, *Quantum computation and quantum information* (Cambridge university press, 2010).
- [38] J. L. Birman, A. A. Maradudin, R. Pick, and K. K. Rebane, Ija Pavlovna Ipatova, *Physics Today* **57**, 69 (2004).
- [39] V. G. Malyshkin, The code for polynomials calculation (2014), <http://www.ioffe.ru/LNEPS/malyshkin/code.html> and an alternative location.